Available online at www.sciencedirect.com

ScienceDirect

Procedia CIRP 117 (2023) 414–419

www.elsevier.com/locate/procedia

19th CIRP Conference on Modeling of Machining Operations

Study on the effect of wear models in tool wear simulation using hybrid SPH-FEM method

Nanyuan Zhang[a,*], Hagen Klippel[a], Fabian Kneubühler[a], Mohamadreza Afrasiabi[b], Matthias Röthlin[c], Michal Kuffa[a], Markus Bambach[d], Konrad Wegener[a]

[a]*Institute of Machine Tools & Manufacturing, D-MAVT, ETH Zürich, Leonhardstrasse 21, 8092 Zurich, Switzerland*
[b]*Data-Driven, & Computational Manufacturing Group, inspire AG, Technoparkstrasse 1, 8005 Zurich, Switzerland*
[c]*Federal Office of Meteorology & Climatology, MeteoSwiss, 8058 Zürich-Airport, Switzerland*
[d]*Advanced Manufacturing Lab, ETH Zürich, Technoparkstrasse 1, 8005 Zurich, Switzerland*

* Corresponding author. Tel.: +41 44 633 07 32. *E-mail address:* zhang@iwf.mavt.ethz.ch

Abstract

The prediction of the tool wear progression using numerical methods has been widely studied in recent years, and various wear models considering different wear mechanisms have been implemented in the simulation work. Typically, these wear models take the physical fields such as contact pressure, sliding velocity and temperature at the tool-workpiece interface into account and are applied either individually or in combinations into the wear simulation. However, how and to what extent the physical parameters in these models affect the generated wear profiles have not been explored in detail in the simulation. In this paper, the behaviors of several typical wear models are studied by simulating the tool wear of cutting Ti6Al4V using a hybrid SPH-FEM method. Considering different combinations of physical contact parameters in the wear model, the simulated wear progression is discussed, and the resulting worn tool geometry is qualitatively compared to the experimental result. Furthermore, insights into the calibration of wear models are proposed.

Keywords: Machining; Simulation; Tool wear; Wear modeling; SPH; FEM;

1. Introduction

Tool wear heavily impacts the cost of the machining process and is of great importance to the manufacturing industries. Recent advances in understanding tool wear under different process conditions, particularly in superalloy machining, are summarized by Sharikay et al. [18].

The experimental wear tests using the trial-and-error method are time-consuming and expensive. In addition, they cannot provide detailed tribological information at the tool-chip contact, since conducting in-situ measurements is difficult without altering the actual process conditions [16]. Instead, using modeling methods is another option and has become increasingly important. Considering different microscopic wear mechanisms, such as abrasive wear, adhesive wear, diffusive wear and chemical wear, various physical or phenomenological models that calculate the local wear rate $\dot{w}$ on the tool surface have been proposed [7]. Based on the thermomechanical conditions on the tool-chip contact such as the sliding speed v_s, normal contact pressure σ_n and temperature T, the wear model is typically represented as

$$\dot{w} = f(\sigma_n, v_s, T, ...) \tag{1}$$

Table 1 lists some of the frequently used models in the literature. With the help of analytical machining models or numerical chip formation simulations, the thermomechanical conditions in Eq. (1) are obtained, and the wear distribution and thus the tool life are approximated straightforwardly.

An advanced wear modeling approach that considers the dynamic interaction between the chip formation and the tool wear progression was developed by Yen et al. [22]. In this method, the progression of tool wear is subdivided into discrete wear increments Δt_{wear}, which are in the range of seconds. Inside each wear increment, the chip formation simulation is performed using the Finite Element Method (FEM), and the thermomechanical states on the tool-chip interface are extracted to calculate the local tool wear rate. The cumulative wear volume is then represented by the displacement of the interface nodes in the

10.1016/j.procir.2023.03.070

FEM mesh, and the updated tool is used for the chip formation simulation in the next wear increment. For about twenty years, this staggered numerical approach has remained unchanged and has been used by many researchers to predict tool wear and tool life [12, 4, 8, 6, 5]. Moreover, the application of wear simulations to develop and calibrate new wear models has also gained attention in recent years [23, 16].

Table 1: Typical wear models and the corresponding wear mechanisms.

Wear model	References	Discussion
$\dot{w} = C_1 v_s$	Rabinowicz et al. [15]	abrasive wear model
$\dot{w} = C_1 v_s \sigma_n$	Archard et al. [2]	power density based mechanical wear model
$\dot{w} = C_1 v_s \sigma_n \exp(-\frac{C_2}{T})$	Usui et al. [21]	abrasive (or adhesive) wear model
$\dot{w} = C_1 \exp(-C_2 v_s \sigma_n)$	Rech et al. [16]	power density based model, obtained by regression
$\dot{w} = C_1 v_s + C_2 \exp(-\frac{C_3}{T})$	Takeyama et al. [20]	addition of abrasive and diffusive wear models
$\dot{w} = C_1 v_s \sigma_n \exp(-\frac{C_2}{T}) + C_3(T) \exp(-\frac{C_4}{T})$	Attanasio et al. [4]	addition of abrasive and diffusive wear models
$\dot{w} = C_1 v_s \exp(-\frac{C_2}{T}) + C_3 \sigma_n \exp(-\frac{C_4}{T})$	Zanger et al. [23]	addition of exponential polynomials by regression

C_1, C_2, C_3 and C_4 are constants in each wear model.

Despite the extensive studies, there are some open questions about this wear simulation approach. First, as most of the implemented wear models are calibrated by critical wear quantities such as the crater depth K_T and the flank wear land width VB, the effect of these models on other wear indicators such as the altering of the cutting edge and the contact length has not been considered. Second, the quality of the tool wear prediction depends on the size of the wear increment. However, a finer wear increment resolution requires more repetitions of the chip formation simulations, which vastly increases the computational cost. Third, some customized treatments are introduced for clearance face wear. Typically, an inclination angle of the flank wear land is artificially prescribed, and the nodal displacements on the clearance face are averaged for a uniform profile [13, 6, 5]. Nevertheless, the simulated flank wear should result from the physical interaction between the tool and workpiece rather than the manual intervention.

In this work, the behavior of various available wear models in numerical wear simulations is investigated for the cutting process of Ti6Al4V. Using a hybrid SPH-FEM solver developed in-house, an efficient wear simulation method is introduced and performed in the context of high-fidelity chip formation simulations. The tool wear profiles simulated with different wear models are qualitatively compared with experimental results, and insights for wear model calibration are proposed.

2. Investigation method

2.1. Setups for the hybrid SPH-FEM cutting simulation

An SPH-FEM coupled two-dimensional orthogonal cutting model which has been presented in [24] is used for the wear simulation. Fig. 1 illustrates the sketch of the cutting simulation model, in which the Ti6Al4V workpiece is discretized into SPH particles for the thermomechanical analysis, while the uncoated cemented carbide tool is treated as a rigid body and modeled with FEM meshes for the heat transfer problem. Different from the traditional FEM chip formation simulations, SPH particles replace the mesh based workpiece in this study to avoid the mesh distortion problem. At the same time, the retained FEM cutting tool provides clearly defined surface geometries of the tool for the local wear representation. The mesh size is roughly 10 µm on the tool's surface, while the SPH particle distance is set to 1.67 µm in the workpiece. This setup leads to 8570 elements in the FEM domain and 419,000 SPH particles in the workpiece. Process parameters and tool geometries are specified in Fig. 1. Note that a cutting speed of 381 m/min is too fast for industrial applications, but is useful for quick computations to illustrate simulation methods.

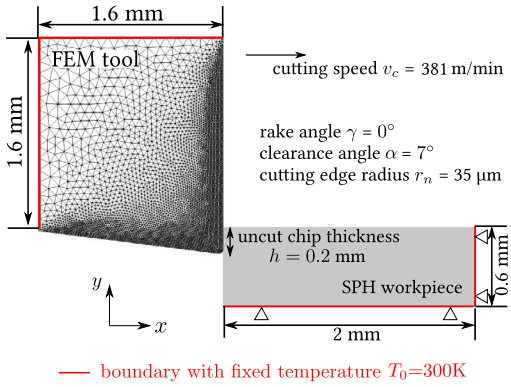

Fig. 1: Configuration of the hybrid SPH-FEM cutting simulation model.

Table 2: Material properties of Ti6Al4V and cemented carbide (grade H13A) used in simulation [1, 9].

Material property	Symbol	Ti6Al4V	Cemented carbide
Density [kg/m^3]	ρ	4430	15250
Young's modulus [GPa]	E	110	-
Poisson ratio [-]	ν	0.35	-
Specific heat [J/(kg·K)]	c_p	526	292
Thermal conductivity [W/(m·K)]	k	6.8	88

The mechanical and thermal properties of workpiece and tool are listed in Table 2. The classic Johnson-Cook (JC) hardening law is implemented to define the plastic behavior of the Ti6Al4V alloy. The material flow stress is given as

$$\sigma_y^{JC} = [A + B(\bar{\epsilon}_{pl})^n][1 + C \ln(\frac{\dot{\bar{\epsilon}}_{pl}}{\dot{\epsilon}_0})][1 - (\frac{T - T_r}{T_m - T_r})^m] \quad (2)$$

where A, B, C, n, m are material constants, $\bar{\epsilon}_{pl}$, $\dot{\bar{\epsilon}}_{pl}$ and $\dot{\epsilon}_0$ are the equivalent plastic strain, equivalent plastic strain rate and reference strain rate respectively. T represents the temperature, while T_m and T_r are the material melting and room temperatures. The values of the JC model for the Ti6Al4V material are taken from [9] and listed in Table 3. The fraction of the plastic work converted into heat, i.e. Taylor-Quinney coefficient is assumed as 0.9 in the model. The establishment of the chip-tool contact between two numerical domains can be found in [24].

Table 3: Johnson-Cook parameters of the workpiece Ti6Al4V [9].

A[MPa]	B[MPa]	C	m	n	T_0[K]	T_m[K]
852	338	0.2754	0.5961	0.148	300	1836

Specifically, the frictional stress τ_f is obtained by the Coulomb friction law with a constant coefficient of friction (COF) value μ. The COF value and other contact parameters including the heat transfer coefficient on the tool-workpiece contact and the frictional heat partition coefficient are given in Table. 4.

Table 4: Contact parameters at tool-workpiece/chip interface in simulation [17].

Contact parameter	Symbol	Value
Heat conduction on interface [W/(m^2·K)]	h_c	$5.0 \cdot 10^6$
Frictional heat partition coefficient to tool [-]	β_{fri}	0.5
Coefficient of friction (COF) [-]	μ	0.35
Conversion of frictional heat [-]	η	1.0

The simulations are conducted on the GPU NVIDIA® Quadro® GP 100 with a runtime of approximately 4 hours. To quickly reach the steady thermal state of the tool-workpiece system, a warm temperature profile is applied to the FEM tool. This profile is obtained by conducting the low resolution simulation with a 10 mm cutting distance such that a steady thermal state in the tool is approximately reached.

2.2. Wear modeling approach

Instead of using the wear increments and conducting the chip formation simulation multiple times, the wear related algorithm is embedded inside a single chip formation simulation in this study. The method is explained in the flowchart in Fig. 2 (a). The modeling approach starts with the thermomechanical calculation of the tool-workpiece system, and the wear related algorithm is activated after a steady thermomechanical state is reached on the tool-chip contact. Afterward, in each time step of the chip formation simulation, the local wear value on the tool surface is computed, and the tool geometry is adjusted by the nodal movement. This indicates that the tool wear progresses simultaneously with the cutting process in the simulation. For a better comparison, the classic wear simulation method explained in Section 1 is presented in Fig. 2 (b).

Nevertheless, the yielded tool wear is limited to the short simulated cutting distance. To acquire the tool wear in a longer cutting period, a scaling factor A is introduced to the implemented wear models. Taking the Usui model as an example, the calculated wear rate at each time step is given as

$$\dot{w} = AC_1\sigma_N v_{rel} \exp\left(-\frac{C_2}{T}\right), \; A \geq 1 \tag{3}$$

where the wear rate $\dot{w}$ is magnified by A times as a result. This implies that for an example with an A of 1000 and the explicit time increment of the chip formation simulation of $1.5 \cdot 10^{-10}$ s, the wear algorithm assumes that the wear rate $\dot{w}$ is constant in 0.15 µs of the tool life. In the end, the simulation of 1 mm cutting distance in the thermal steady state thus corresponds approximately to the tool wear of 1 m cutting length. Naturally, a smaller A is advantageous to accurately track the change in wear rate and the resulting wear profile.

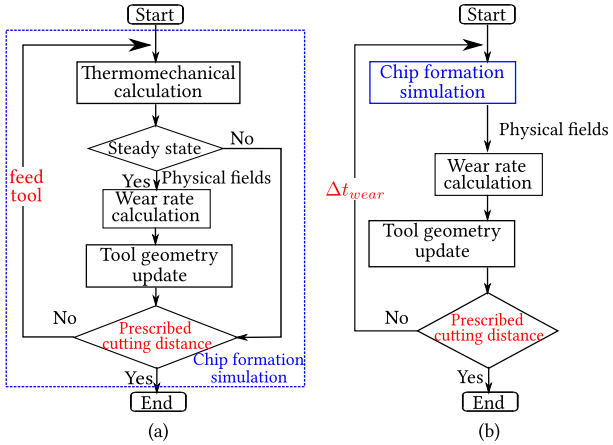

Fig. 2: Comparison of the wear simulation strategies. (a) The in-house developed wear simulation within a chip formation simulation. (b) The traditional modeling approach with wear increments Δt_{wear} and multiple chip formation simulations.

The benefits of this new method are summarized as follows. On the one hand, the computational time is largely reduced as only one chip formation simulation is performed. On the other hand, the worn tool geometry and the chip formation process are more closely interacted, which promotes relatively smooth micro geometries on both the rake and clearance faces of the tool. Therefore, special treatments such as averaging the FEM nodes on the flank wear land [6, 13] are not required in this work.

2.3. Design of numerical tests

There are two major issues when directly comparing the effects of the available wear models. On the one hand, the available wear models are calibrated by different methods, such as the tribometer test [16] or the inverse simulation-cutting experiment approach [6]. With non-identical tribological conditions during the calibration, these wear models can give different results in predicting tool wear for the same machining process. On the other hand, some phenomenological wear models, especially those in an additive form such as the Zanger model are established through regression analysis, and the effect of individual items remains unclear. The influences of these models on the wear progression must therefore be carefully inspected. Consequently, 13 dummy models in the form of polynomial and exponential expressions that compose the wear models in Table 1 are chosen for investigation in this study. The list of these dummy models can be found in Table 5, in which models 1-3 are purely mechanically based and only consider σ_n and v_s, while models 4-13 further involve the temperature influence. As C_1 is unknown in each dummy wear model, the scaling factor A is adjusted flexibly to linearly control the wear rate or the simulated cutting distances. In this way, the specified VB value can be achieved in the simulation, and the generated wear result thus provides information about the behavior of the individual dummy models. The choices of the model constant within the

temperature-dependent exponential term include 2500, 5000, and 10000, which roughly cover the typical values in the literature [22, 12, 6, 5]. It is important to note that mechanisms such as adhesive and diffusive wear are prevalent when machining Ti6Al4V with uncoated carbide tools [11]. Under this circumstance, dummy models 4-10 may be more suitable to apply in this study. Nevertheless, it is worthwhile to investigate the behavior of other wear models in Table 1 to compare the extent to which the inclusion of each physical variable has an impact.

Table 5: Tested dummy wear models with polynomial and exponential terms.

No.	Dummy wear model	σ_n	v_s	T	Representation
1	$\dot{w} = C_1 v_s$		✓		Abrasive wear model
2	$\dot{w} = C_1 v_s \sigma_n$	✓	✓		Archard wear model
3	$\dot{w} = C_1 \exp(8\text{E-}10 v_s \sigma_n)$	✓	✓		Rech wear model
4	$\dot{w} = C_1 v_s \sigma_n \exp(-\frac{2500}{T})$	✓	✓	✓	Usui wear model
5	$\dot{w} = C_1 v_s \sigma_n \exp(-\frac{5000}{T})$	✓	✓	✓	Usui wear model
6	$\dot{w} = C_1 v_s \sigma_n \exp(-\frac{10000}{T})$	✓	✓	✓	Usui wear model
7	$\dot{w} = C_1 \exp(-\frac{2500}{T})$			✓	Diffusive wear model
8	$\dot{w} = C_1 \exp(-\frac{5000}{T})$			✓	Diffusive wear model
9	$\dot{w} = C_1 \exp(-\frac{10000}{T})$			✓	Diffusivei wear model
10	$\dot{w} = C_1 v_s \exp(-\frac{2500}{T})$		✓	✓	Zanger wear model
11	$\dot{w} = C_1 v_s \exp(-\frac{5000}{T})$		✓	✓	Zanger wear model
12	$\dot{w} = C_1 v_s \exp(-\frac{10000}{T})$		✓	✓	Zanger wear model
13	$\dot{w} = C_1 \sigma_n \exp(-\frac{10000}{T})$	✓		✓	Zanger wear model

2.4. Validating experiments

The quasi-orthogonal machining experiment is performed by longitudinal turning of a hollow cylindrical Ti6Al4V workpiece on the Schaublin 42L CNC lathe. The detailed conditions of the workpiece and tool materials can be found in [10]. The process parameters are set as they are listed in the Fig. 1, and no coolant or lubricant is used in the experiments. After 1.2 m cutting distance, the cross section of the tool is examined with a confocal microscope, and the measured profile is qualitatively compared with the simulated results in the next section.

3. Results and discussions

3.1. Simulated physical variables on the tool-chip contact

The simulated thermomechanical conditions and the relative wear rate are illustrated in Fig. 3, where the results for both the new and worn tool with dummy model 5 are compared. Even though the physical variables may vary due to the serrated chip morphology, some discoveries can be generalized as follows. The sliding velocity v_s tends to zero around the cutting edge and increases along the contact on the rake face. On the contrary, σ_n has its peak value around the cutting edge and decreases along the rake face to the end of the contact. Consequently, the power density, i.e. the multiplication of the normal contact pressure and sliding velocity $\sigma_n v_s$, varies on the contact with its maximum value located in the middle of the rake face. Although the temperature varies along the rake surface, its difference does not exceed 25% along the contact. Thus, the variation of the wear rate on the tool's surface closely follows the power density, with its amplitude locally adjusted by the surface temperature. The simulated contact length increases with the tool wear progression on the rake face. This phenomenon may explain the underestimation of the contact length in machining simulations reported by Arrazola et al. [3], as the effect of the worn tool geometry is rarely considered in the numerical models.

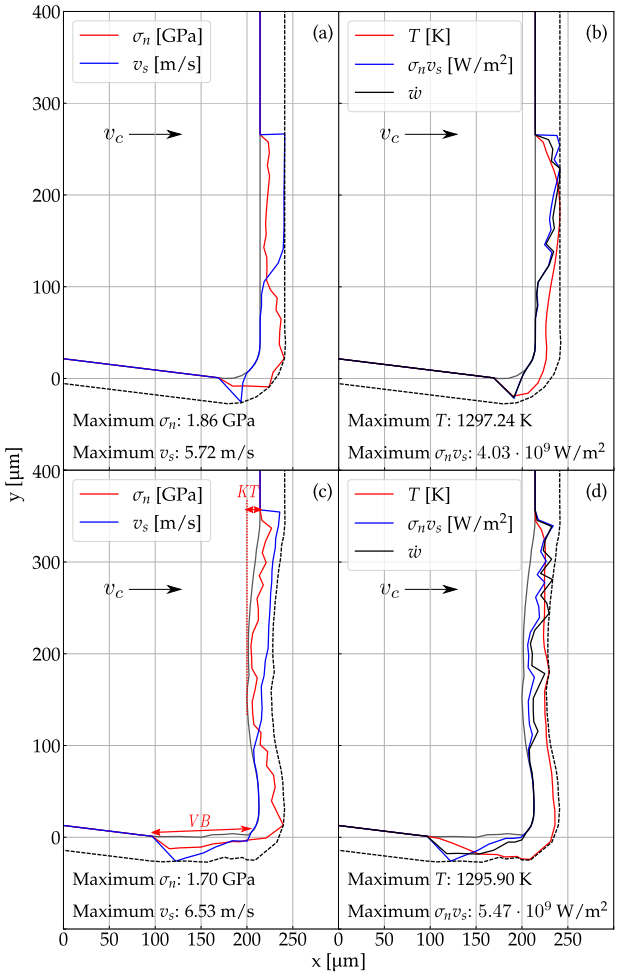

Fig. 3: Simulated thermomechanical conditions and wear rates on the tool-chip and tool-machined workpiece contact using dummy model 5. (a) and (b) represent the result at the initial stage of the wear process, while (c) and (d) represent the result when VB roughly reaches 100 µm. The local wear rate $\dot{w}$ is normalized to show the variation trend. The dashed line denotes the scale of the maximum physical value in each figure, while the solid line represents the tool surface and indicates zeros of σ_n, v_s, $\sigma_n v_s$ and $\dot{w}$, and 1000 K of T as baselines.

3.2. Comparison of dummy wear models

Since VB is often used in the literature as a criterion for calibrating wear models, the wear results of each dummy model in Table 5 are compared with the experimentally measured tool profile in Fig. 4 when VB = 100 µm is approximately reached. Particularly, the wear progression with dummy models 1, 6, 9 and 12 are illustrated in Fig. 5, where the tool profiles are given according to equidistant cutting lengths for a qualitative comparison, and the distance between two adjacent profile lines reflects the local wear rate. Although all of the dummy wear models are able to deliver the flank and crater wears, none of the models accurately capture the measured contours of the worn

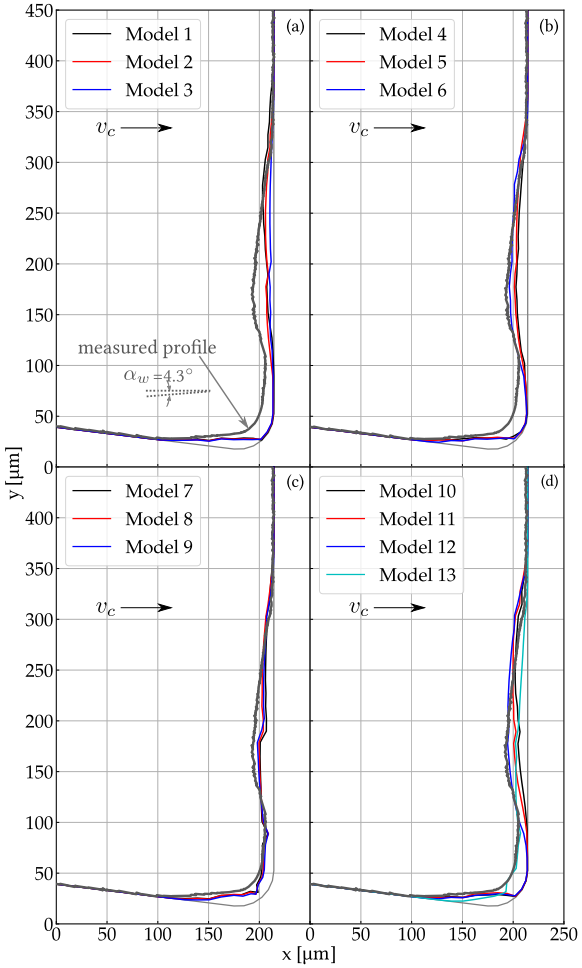

Fig. 4: Simulated worn tool profiles using different dummy wear models and the measured tool profile from the cutting test. (a) mechanical wear models (dummy models 1, 2 and 3), (b) Usui wear models (dummy models 4, 5 and 6), (c) diffusive wear models (dummy models 7, 8 and 9), (d) components in Zanger wear model (dummy models 10, 11, 12 and 13).

tool. Differences can be observed in the inclination angle α_w of the flank wear land, the crater depth, and the worn cutting edge.

When the mechanical wear models (dummy models 1, 2 and 3 in Fig. 4 (a)) are implemented in the simulation, the part of the rake face which is close to the cutting edge remains nearly unworn, and shallower craters are formed compared to other wear modeling results. Especially, for the result with dummy model 1 (abrasive wear law [15]) in which only v_s is considered in the model, the simulated flank wear land is nearly parallel to the cutting direction, and the cutting tool seems to exhibit a "self-sharpening" effect in Fig. 5 (a). Although such a tendency cannot be verified for titanium alloy machining, a similar pattern has been found in the machining of carbon-fiber-reinforced polymer, where the abrasive wear dominates [19].

As the temperature is further included in wear modeling, i.e. dummy models 4-6 (the Usui wear model) and 10-12 (the first term of the Zanger wear model), the results given in Fig. 4 (b) and (d) present deeper craters on the rake face. Similar to the purely mechanically based wear models without considering the temperature, the Usui and the first item of the Zanger wear models are not able to yield significant wear around the cutting edge. The flank wear land is formed with a small inclination angle α_w upward in the cutting direction. As shown in Fig. 5, this angle appears to be stable during the wear progression. In addition, due to the variation of the constant value in the exponential polynomials, the amplitudes of KT are slightly different inside the model group 4-6 and 10-12, although the location of maximum crater depth does not vary significantly. This might indicate that the inclusion of the exponential temperature term in either the Usui model or the first item of the Zanger wear model can further regulate the wear rate on the tool surface. A similar effect has also been reported by Methon et al. [14]. Nevertheless, it is unclear whether the sliding power or the temperature plays a decisive role in the dummy models 4-6 and 10-12, since the temperature distribution on the rake face correlates strongly with the frictional energy and thus v_s. For the wear progression in Fig. 5 (b) and (d), the wear rate of the rake face appears to be stable. However, the expansion of the flank wear land shows a decreasing tendency in Fig. 5 (b) based on the densification of the subsequential profile lines on the clearance face. One explanation could be that the expanded flank wear land reduces the normal surface pressure.

Special attention should be paid to dummy models 7-9, i.e. the diffusive wear model, which induces significant wear around the cutting edge and forms shallower craters as shown in Fig. 4 (c) than the results with dummy models 4-6 and 10-12. The additional inclusion of σ_n in the diffusive model further promotes the cutting edge wear, which can be referred to the worn tool profile using dummy model 13 in Fig. 4 (d). Since T is the only influencing parameter of the diffusive wear model, the worn tool profiles reflect the temperature distribution on the tool surface. As models 7, 8 and 9 nearly yield identical wear profiles when $VB = 100$ µm is reached, it can be deduced that a unique set of constants in the diffusion wear model cannot be determined by inverse calibration work using simulations. Instead, the analytical approach, which is on the basis of the material transfer across the interface, should be used to derive the diffusive wear model. Besides, Fig. 5 (c) shows that the wear rates on the clearance and rake faces appear to be unchanged when the diffusive dummy model 8 is implemented. This can be explained by the nearly stable temperature at the contact during the simulation.

It can be deduced that to obtain the crater wear together with the worn cutting edge simultaneously, it is advisable to combine the diffusive wear model with other mechanically based models such as the Usui model in the simulation. In this case, the measured worn tool geometries can be closely reproduced. Such model selection in turn also indirectly verifies the main wear mechanisms of Ti6Al4V machining, i.e. the adhesive wear and diffusive wear [11].

4. Conclusion

This paper presents an efficient approach of tool wear simulation using the coupled numerical SPH-FEM method. With 13 dummy models, the influences of the physical quantities in the typical wear models are investigated and the simulated wear

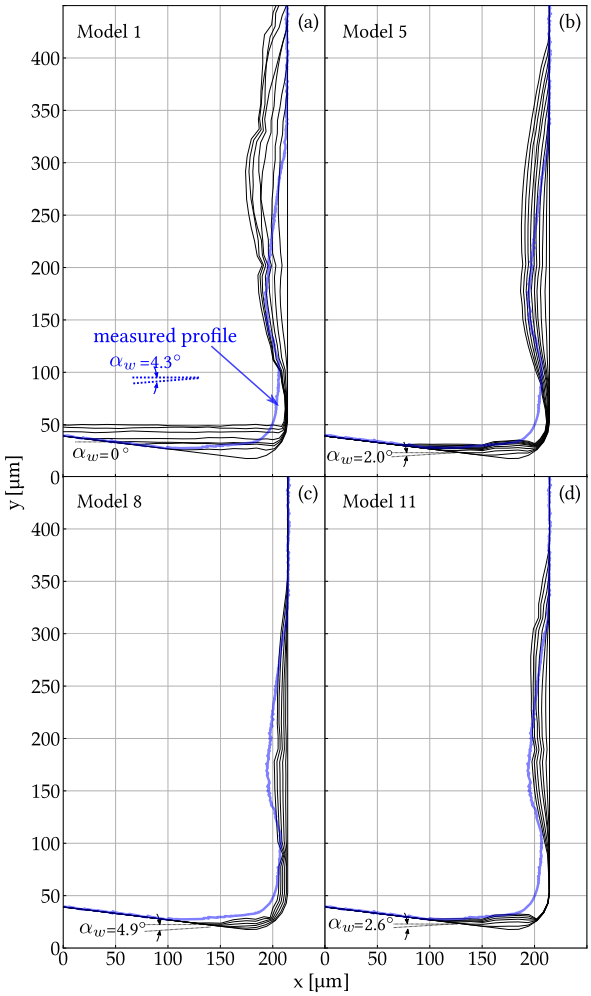

Fig. 5: Simulated wear progression with (a) abrasive wear model, (b) Usui wear model, (c) diffusive wear model and (d) first item of Zanger wear model.

indicators such as flank wear land, crater depth and worn cutting edge are qualitatively compared. Based on the simulated wear profiles, knowledge is gained for the future identification of wear model parameters. Since different wear models lead to different wear patterns, the simulated tool wear profiles can in turn provide practical indications of the main wear mechanisms in experimentally acquired tool profiles.

It has been revealed that using a single wear model in the simulation often fails to predict the correct tool wear profile for all of the above indicators simultaneously. Therefore, the use of a model with an additive form might be considered a sufficient condition for the correct representation of the wear in the simulation. Nevertheless, the necessity of such an approach needs to be further validated. Future research should focus on the calibration of wear models and the interaction of friction and tool wear at the tool-chip contact interface.

References

[1] Afrasiabi, M., Meier, L., Röthlin, M., Klippel, H., Wegener, K., 2020. GPU-accelerated meshfree simulations for parameter identification of a friction model in metal machining. International Journal of Mechanical Sciences 176, 105571.

[2] Archard, J., 1953. Contact and rubbing of flat surfaces. Journal of applied physics 24, 981–988.

[3] Arrazola, P., Ugarte, D., Dominguez, X., 2008. A new approach for the friction identification during machining through the use of finite element modeling. International Journal of Machine Tools and Manufacture 48, 173–183.

[4] Attanasio, A., Ceretti, E., Fiorentino, A., Cappellini, C., Giardini, C., 2010. Investigation and FEM-based simulation of tool wear in turning operations with uncoated carbide tools. Wear 269, 344–350.

[5] Bencheikh, I., Nouari, M., Bilteryst, F., 2020. Multi-step simulation of multi-coated tool wear using the coupled approach XFEM/multi-level-set. Tribology International 146, 106034.

[6] Binder, M., Klocke, F., Döbbeler, B., 2017. An advanced numerical approach on tool wear simulation for tool and process design in metal cutting. Simulation modelling practice and theory 70, 65–82.

[7] Childs, T.H., Maekawa, K., Obikawa, T., Yamane, Y., 2000. Metal machining: theory and applications. Butterworth-Heinemann.

[8] Haddag, B., Nouari, M., 2013. Tool wear and heat transfer analyses in dry machining based on multi-steps numerical modelling and experimental validation. Wear 302, 1158–1170.

[9] Klippel, H., 2021. Constitutive equations for simulation of metal cutting with meshless methods on GPU. Ph.D. thesis. ETH Zurich.

[10] Klippel, H., Süssmaier, S., Kuffa, M., Wegener, K., 2022. Dry cutting experiments database Ti6Al4V and Ck45.

[11] Lindvall, R., Lenrick, F., M'Saoubi, R., Ståhl, J.E., Bushlya, V., 2021. Performance and wear mechanisms of uncoated cemented carbide cutting tools in Ti6Al4V machining. Wear 477, 203824.

[12] Lorentzon, J., Järvstråt, N., 2008. Modelling tool wear in cemented-carbide machining alloy 718. International Journal of Machine Tools and Manufacture 48, 1072–1080.

[13] Malakizadi, A., Gruber, H., Sadik, I., Nyborg, L., 2016. An FEM-based approach for tool wear estimation in machining. Wear 368, 10–24.

[14] Methon, G., Courbon, C., M'Saoubi, R., Girinon, M., Rech, J., 2022. Tribological considerations when modelling tool wear in turning of 15-5PH stainless steel, in: Defect and Diffusion Forum, Trans Tech Publ. pp. 33–38.

[15] Rabinowicz, E., Dunn, L., Russell, P., 1961. A study of abrasive wear under three-body conditions. wear 4, 345–355.

[16] Rech, J., Giovenco, A., Courbon, C., Cabanettes, F., 2018. Toward a new tribological approach to predict cutting tool wear. CIRP Annals 67, 65–68.

[17] Röthlin, M., Klippel, H., Afrasiabi, M., Wegener, K., 2019. Metal cutting simulations using smoothed particle hydrodynamics on the GPU. The International Journal of Advanced Manufacturing Technology 102, 3445–3457.

[18] Sarıkaya, M., Gupta, M.K., Tomaz, I., Pimenov, D.Y., Kuntoğlu, M., Khanna, N., Yıldırım, Ç.V., Krolczyk, G.M., 2021. A state-of-the-art review on tool wear and surface integrity characteristics in machining of superalloys. CIRP Journal of Manufacturing Science and Technology 35, 624–658.

[19] Seeholzer, L., Krammer, T., Saeedi, P., Wegener, K., 2022. Analytical model for predicting tool wear in orthogonal machining of unidirectional carbon fibre reinforced polymer (CFRP). The International Journal of Advanced Manufacturing Technology 119, 7259–7289.

[20] Takeyama, H., Murata, R., 1963. Basic investigation of tool wear. Journal of Engineering for Industry 78, 33–38.

[21] Usui, E., Shirakashi, T., Kitagawa, T., 1978. Analytical prediction of three dimensional cutting process—Part 3: Cutting temperature and crater wear of carbide tool .

[22] Yen, Y.C., Söhner, J., Weule, H., Schmidt, J., Altan, T., 2002. Estimation of tool wear of carbide tool in orthogonal cutting using FEM simulation. Machining science and technology 6, 467–486.

[23] Zanger, F., Schulze, V., 2013. Investigations on mechanisms of tool wear in machining of Ti-6Al-4V using FEM simulation. Procedia CIRP 8, 158–163.

[24] Zhang, N., Klippel, H., Afrasiabi, M., Röthlin, M., Kuffa, M., Bambach, M., Wegener, K., 2023. Hybrid SPH-FEM solver for metal cutting simulations on the GPU including thermal contact modeling. CIRP Journal of Manufacturing Science and Technology 41, 311–327.